

## Topological Structures of Energy Flow: Poynting Vector Skyrmions


Sicong Wang, Zhikai Zhou<sup>✉</sup>, Zecan Zheng, Jialin Sun, Hongkun Cao,

Shichao Song, Zi-Lan Deng, Fei Qin, Yaoyu Cao, and Xiangping Li<sup>✉\*</sup>

*Guangdong Provincial Key Laboratory of Optical Fiber Sensing and Communications,*

*Institute of Photonics Technology, Jinan University, Guangzhou 510632, China*

*and College of Physics & Optoelectronic Engineering, Jinan University, Guangzhou 510632, China*

 (Received 14 March 2023; revised 29 May 2024; accepted 16 July 2024; published 14 August 2024)

Topological properties of energy flow of light are fundamentally interesting and may introduce novel physical phenomena associated with directional light scattering and optical trapping. In this Letter, skyrmionlike structures formed by Poynting vectors are unveiled in the focal region of two pairs of counterpropagating cylindrical vector vortex beams in free space. The appearance of local phase singularities, and the distinct traveling and standing wave modes of different field components passing through the focal spot lead to a Néel-Bloch-Néel transition of Poynting vector skyrmion textures along the light propagating direction. By shaping the wave front of the incident beams with patterned amplitudes, the topological invariant of the Poynting vector skyrmions can be further tuned in a prospective area. This work expands the family of optical skyrmions and holds great potential in energy flow associated applications.

DOI: [10.1103/PhysRevLett.133.073802](https://doi.org/10.1103/PhysRevLett.133.073802)

Skyrmions acting as a typical branch of topologically nontrivial textures were originally proposed by Skyrme [1] and have been demonstrated in Bose-Einstein condensates [2,3], nematic liquid crystals [4], and as a phase transition in chiral magnets [5,6]. Especially, magnetic skyrmions have been extensively studied and considered as promising routes toward high-density magnetic information storage, transfer, and spintronic devices [7–9]. Recently, optical skyrmions have sprung up and expanded the family of skyrmions [10]. Different types of optical skyrmions formed by electromagnetic field [11–15], spin [16–21], or Stokes vectors [22–25] have been demonstrated by the interference of propagating surface plasmons on a metal surface or by the interference of structured light in free space, which greatly enriched the research field of topological optics. Furthermore, spin manipulation in an optical skyrmion pair has been applied in a metrology system, which is capable of attaining picometric sensitivity to displacements [26]. This makes a good start for real applications of optical skyrmions.

As another fundamental quantity, Poynting vector describes the magnitude and direction of the energy flow of light. It plays an important role in light scattering [27] and optical force [28,29]. For example, in an optical tweezer system, the motion trajectory of an absorbing particle coincides with the orientation of the energy flow, and the velocity of the particle motion is proportional to the corresponding flow modulus [30–32]. With the development of vector beams, complex behaviors of energy flow are

unveiled under tight focusing conditions. Transversal toroidal energy flow [33–35], longitudinal energy backflow [36–40], and topological structures of energy flow [14,41,42], for example, the fractal-like energy flow of supertoroidal light pulses, have been studied. Instinctively, energy flow with skyrmionlike topological structures may further enrich light-matter interactions with its unique vector distribution and expand the family of optical skyrmions.

In this Letter, optical skyrmions formed by Poynting vectors are theoretically demonstrated in the focal region of two pairs of counterpropagating cylindrical vector vortex beams in free space. A Néel-Bloch-Néel transition of Poynting vector skyrmion textures is observed along the light propagating direction within a subwavelength focal volume. Through further modulating the amplitude of the incident beams, the topological invariant of the Poynting vector skyrmions can be tuned in a prospective area.

As shown in Fig. 1, two pairs of counterpropagating cylindrical vector vortex beams, one with azimuthally polarized electric field  $\mathbf{E}$  and radially polarized magnetic field  $\mathbf{H}$  (Parts I and III), and the other one with radially polarized electric field  $\mathbf{E}$  and azimuthally polarized magnetic field  $\mathbf{H}$  with a phase delay of  $\pi/2$  supplied by a homogeneous phase plate (PP1 and PP2) (Parts II and IV), are focused through a  $4\pi$  focal system.  $\mathbf{E}$ ,  $\mathbf{H}$ , and their propagating direction satisfy right-handed spiral relationship. It can be inferred that the transversal and the longitudinal components of the total electric field in the focal plane can be modulated independently by Parts I + III and Parts II + IV, respectively, and vice versa for the magnetic field. Considering the stability of light beams during propagation, superposition of different types of

\*Contact author: [xiangpingli@jnu.edu.cn](mailto:xiangpingli@jnu.edu.cn)

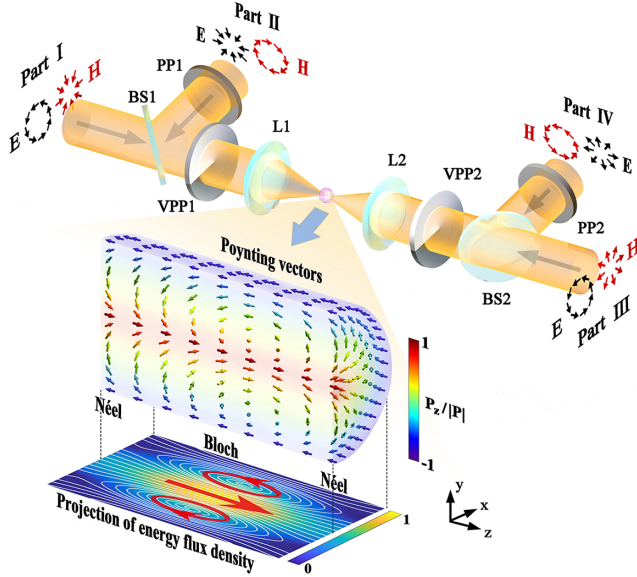


FIG. 1. Schematic of the generation of Poynting vector skyrmions in the focal region of two pairs of counterpropagating cylindrical vector vortex beams. The Poynting vectors experience a Néel-Bloch-Néel transition of skyrmion textures along the light propagating direction. The red arrows below indicate the directions of the projection of energy flux density.

Laguerre-Gauss modes is usually suggested to describe incident beams [43]. In this manner, higher-order vortex beams with vector polarizations have been successfully constructed [44]. However, for simplicity, in our configuration the first-order vortex phases are introduced by the vortex phase plates (VPP1 and VPP2) placed directly at the back apertures of the focal lenses, through which the incident beams are focused immediately. This focusing manner has been widely adopted for many scenarios to investigate other optical structures, such as superoscillatory focal spots, optical needles, and optical skyrmions, which have been theoretically generated by encoding more complex phase and polarization distributions to the incident beams [15,39,45,46]. In simulation, equivalent and uniformly distributed light intensity is assumed for the two pairs of incident beams, except for the polarization singularity in the center where the light intensity is zero. The enlarged view denotes the schematic of the Néel-Bloch-Néel transition of skyrmion textures along the light propagating direction.

According to the Richards-Wolf diffraction theory [47] and the characteristics of the field superposition of a  $4\pi$  focal system [48–50], the electromagnetic field in the focal region can be expressed as

$$\mathbf{E}_f(r, \varphi, z) = Ae^{i\varphi} \int_0^{\theta_{\max}} \begin{bmatrix} V_1 W_1 + V_2 W_2 \cos \theta \\ i(V_2 W_1 + V_1 W_2 \cos \theta) \\ -2iV_3 W_1 \sin \theta \end{bmatrix} \begin{bmatrix} \mathbf{e}_r \\ \mathbf{e}_\varphi \\ \mathbf{e}_z \end{bmatrix} \times T d\theta, \quad (1)$$

$$\mathbf{H}_f(r, \varphi, z) = -\frac{iA}{\mu_0 c} e^{i\varphi} \int_0^{\theta_{\max}} \begin{bmatrix} V_1 W_1 + V_2 W_2 \cos \theta \\ i(V_2 W_1 + V_1 W_2 \cos \theta) \\ -2iV_3 W_1 \sin \theta \end{bmatrix} \begin{bmatrix} \mathbf{e}_r \\ \mathbf{e}_\varphi \\ \mathbf{e}_z \end{bmatrix} \times T d\theta, \quad (2)$$

where

$$\begin{aligned} V_1 &= J_0(kr \sin \theta) + J_2(kr \sin \theta), \\ V_2 &= J_0(kr \sin \theta) - J_2(kr \sin \theta), \\ V_3 &= J_1(kr \sin \theta), \end{aligned} \quad (3)$$

and

$$\begin{aligned} W_1 &= e^{ikz \cos \theta} + e^{-ikz \cos \theta}, \\ W_2 &= e^{ikz \cos \theta} - e^{-ikz \cos \theta}, \\ T &= \sqrt{\cos \theta} \sin \theta, \end{aligned} \quad (4)$$

$r$ ,  $\varphi$ , and  $z$  are the cylindrical coordinates in the focal region.  $\theta$  is the converging angle, which varies from 0 to  $\theta_{\max}$ .  $\theta_{\max} = \arcsin(\text{NA})$  is the maximum converging angle of the focal lens, and  $\text{NA} = 0.95$  is the corresponding numerical aperture.  $A$  is a complex constant.  $\mu_0$  is the permeability of vacuum and  $c$  is the speed of light in vacuum.  $\mathbf{e}_r$ ,  $\mathbf{e}_\varphi$ , and  $\mathbf{e}_z$  are the unit base vectors.  $k$  is the wave number of the beams.  $J_0$ ,  $J_1$ , and  $J_2$  denote the Bessel functions of the first kind. More detailed formula derivations are shown in Supplemental Material, Note 1 [51]. From Eqs. (1) and (2), it can be seen that, except for a phase delay of  $3\pi/2$  or a phase lead of  $\pi/2$ , the focal magnetic field  $\mathbf{H}_f$  has the same normalized field distributions with the focal electric field  $\mathbf{E}_f$ . Subsequently, the Poynting vector, namely the energy flux density, of the electromagnetic field in the focal region can be calculated through  $\mathbf{P}(r, \varphi, z) = 1/2\text{Re}(\mathbf{E}_f \times \mathbf{H}_f^*)$ , where  $\mathbf{H}_f^*$  is the conjugate of  $\mathbf{H}_f$ .

The whole picture of the generated Poynting vector skyrmions is shown in Fig. 2. Figure 2(a) shows the normalized amplitude and the unit vector projections of the Poynting vectors on the  $x$ - $y$  plane at different longitudinal positions. Each subfigure is normalized to itself. Within the red circles, complete skyrmion structures are formed. Their three-dimensional vectorial structures formed by unit vectors are shown in Fig. 2(b). It can be seen that the Poynting vectors reverse from the “up” state in the center to the “down” state at the periphery with different skyrmion types. Figure 2(c) illustrates the normalized cross sections of the individual components of the Poynting vector skyrmions. It can be perceived that the azimuthal component  $P_\varphi$  decreases gradually and outward-pointing radial component  $P_r (> 0)$  emerges from  $z = 0$  to

$z = 0.35\lambda$ . Inversely, inward-pointing radial component  $P_r(<0)$  emerges from  $z = 0$  to  $z = -0.35\lambda$ . At  $z = \pm 0.35\lambda$ ,  $P_\phi$  is almost vanishing in the central region and the corresponding purity of the local Poynting vector components in the  $r$ - $z$  plane ( $P_r$  and  $P_z$ ), calculated by  $(|P_r|^2 + |P_z|^2)/(|P_r|^2 + |P_\phi|^2 + |P_z|^2)$  remains higher than 97% within the whole skyrmion region, which is illustrated in Supplemental Material, Fig. S1 [51]. These results indicate that a Néel-Bloch-Néel transition of skyrmion textures can be observed along the light propagating direction. The handedness of the Bloch-type Poynting vector skyrmion can be reversed by introducing an additional phase of  $\pi$  to Parts II and IV.

$P_z/|\mathbf{P}|$  is the cosine of the orientation angle of the Poynting vector with respect to the  $z$  axis. Figure 2(d) shows the variation of  $P_z/|\mathbf{P}|$  along the radial direction from the center to the periphery. It illustrates that  $P_z/|\mathbf{P}|$  varies monotonically from 1 at  $r = 0$  to  $-1$  at the periphery within the pink shadow area. If  $|z| > 0.35\lambda$ , for example  $|z| = 0.4\lambda$ ,  $P_z/|\mathbf{P}|$  does not vary monotonically any more as indicated by the red circle and hence breaks the skyrmion structure.

The skyrmion number ( $N_{\text{sk}}$ ) can be written in an integral form [8,11,16]

$$N_{\text{sk}} = \frac{1}{4\pi} \iint_S n dS = \frac{1}{4\pi} \iint_S \mathbf{e}_p \cdot \left( \frac{\partial \mathbf{e}_p}{\partial x} \times \frac{\partial \mathbf{e}_p}{\partial y} \right) dx dy, \quad (5)$$

where the area  $S$  covers the complete Poynting vector skyrmion and  $n$  is the skyrmion number density.  $\mathbf{e}_p$  represents the unit vector in the direction of the local Poynting vector. The skyrmion numbers within the range  $|z| \leq 0.35\lambda$  are calculated and shown in Fig. 2(e), all of which are almost equal to 1. The deviations from 1 stem from calculation errors.

The normalized amplitude and the unit vector projections of the Poynting vectors on the  $r$ - $z$  plane are shown in Fig. 2(f). From the enlarged area indicated by the red square, changes of the azimuthal component of the Poynting vectors, namely the transition between the black arrows and the black dots along the  $z$  direction, can be seen. This changing regularity is consistent with the Néel-Bloch-Néel type transition of the Poynting vector skyrmions along

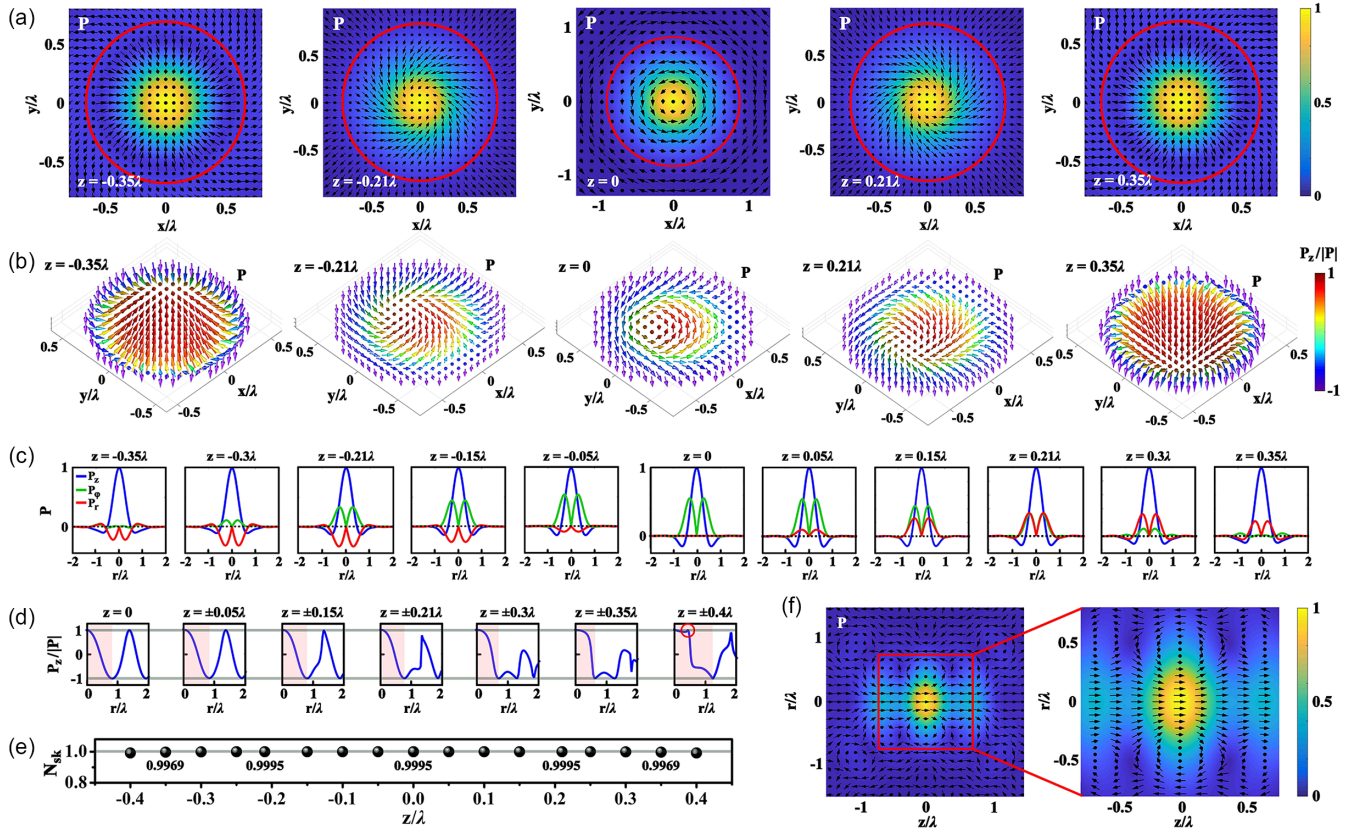


FIG. 2. Simulated results of the Poynting vector skyrmions. (a) The normalized amplitude and the unit vector projections of the Poynting vectors on the  $x$ - $y$  plane at different longitudinal positions. Each subfigure is normalized to itself. (b) The three-dimensional vectorial structures of the Poynting vector skyrmions formed by unit vectors within the red circles in (a). (c) The normalized cross sections of the individual components of the Poynting vector skyrmions. Each subfigure is normalized to itself. (d) Variations of  $P_z/|\mathbf{P}|$  versus  $r$ . (e) Skyrmion numbers at different longitudinal positions. (f) The normalized amplitude and the unit vector projections of the Poynting vectors on the  $r$ - $z$  plane.



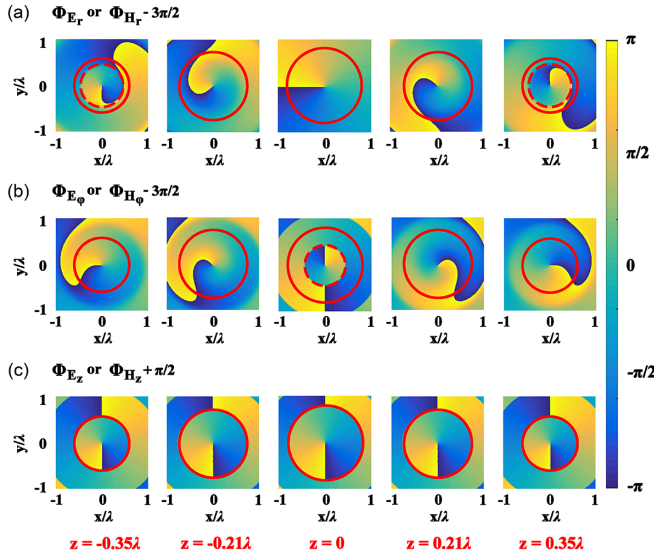


FIG. 3. The phase distributions of the individual field components in the  $x$ - $y$  plane at different longitudinal positions. (a) The phase distributions of  $E_r$  and  $H_r$ . (b) The phase distributions of  $E_\phi$  and  $H_\phi$ . (c) The phase distributions of  $E_z$  and  $H_z$ . The solid red circles indicate both the singular lines of  $E_z(H_z)$  and the areas within which complete Poynting vector skyrmions are formed. The dashed red circles indicate the singular lines of  $E_r(H_r)$  or  $E_\phi(H_\phi)$ .

the light propagating direction. The normalized energy density of the electromagnetic field in the focal region are shown in Supplemental Material, Fig. S2 [51].

To further explain the skyrmion texture transition, phase distributions of the individual field components in the  $x$ - $y$  plane at different longitudinal positions are analyzed as shown in Fig. 3. All of the field components are encoded with a vortex phase with a topological charge of 1. The polarization in the center is circular polarization, which has been discussed in Ref. [52]. It can be seen that  $\mathbf{H}_f$  has a phase delay of  $3\pi/2$  or a phase lead of  $\pi/2$  compared with  $\mathbf{E}_f$ . The vortex phases of  $E_r(H_r)$  and  $E_\phi(H_\phi)$  rotate clockwise from  $z = -0.35\lambda$  to  $z = 0.35\lambda$ , while that of  $E_z(H_z)$  remains unchanged. This implies that the transversal components evolve as traveling waves, while the longitudinal component performs as a standing wave. This is due to the polarization asymmetry of the counterpropagating incident beams. They are not mirrorsymmetric with respect to the focal plane, which can be perceived more straightforwardly in Fig. S3 [51]. The polarization handedness of the counterpropagating incident beams is opposite when observing along the  $z$  axis. As for the longitudinal components,  $E_z(H_z)$  is generated by Parts II + IV (Parts I + III) only. In this case, there is only a  $\pi$  phase difference between the counterpropagating radially polarized incident fields, and hence the generated focal field is a standing wave with a position shift compared to that generated by

mirrorsymmetric incident beams. The dependence of the phases of  $E_r(H_r)$  and  $E_\phi(H_\phi)$ , and the independence of the phase of  $E_z(H_z)$  on the longitudinal position  $z$  can be also verified by Eqs. (1)–(4) analytically. During the phase rotation of the transversal components, the vortex phase of  $E_\phi(H_\phi)$  keeps delayed by  $\pi/2$  compared with  $E_r(H_r)$  and these vortex phases experience a change of  $\pi/2$  from  $z = 0$  to  $z = \pm 0.35\lambda$ . This changing regularity boosts the skyrmion texture transition of the Poynting vectors along the light propagating direction, which can be understood by analyzing the individual components of the Poynting vectors in this phase changing process.

On the other hand, phase singularities are ubiquitous phenomena in the interference of multiple electromagnetic waves and provide additional insights into propagation and interaction of electromagnetic waves [28]. In our case, through the interference of two pairs of counterpropagating cylindrical vector vortex beams, phase singularities emerge for all of the field components and result in zero amplitude distributions in the corresponding regions. As shown in Fig. 3, the solid red circles indicate both the singular lines of  $E_z(H_z)$  and the areas within which complete Poynting vector skyrmions are formed. Along these solid circles,  $E_z$  and  $H_z$  vanish and the other field components will only result in Poynting vectors with the longitudinal orientation ( $P_z$ ). Similarly, as indicated by the dashed red circles in Figs. 3(a) and 3(b), when passing through the focal spot, the alternate appearance of the local phase singularities of  $E_r(H_r)$  and  $E_\phi(H_\phi)$  will lead to the alternate suppression of  $P_\phi$  and  $P_r$ . These phase singularities determine the spatial sizes of the Poynting vector skyrmions and contribute to the skyrmion texture transition along the light propagating direction.

The local singularities can also be achieved and modulated through wave front shaping of incident beams, which provides an effective means to tune topological invariants of the Poynting vector skyrmions. In Figs. 4(a1)–4(a3), we demonstrate that three types of amplitude modulation rings can be used to generate Poynting vector skyrmions with certain skyrmion numbers.  $R_0$  is the radius of the back aperture of the focal lenses.  $R_i$ ,  $R_{i1}$ , and  $R_{i2}$  are the inner radii of the amplitude modulation rings. The radius ratios of the three modulation rings are 0.68:1, 0.3:0.83:1, and 0.88:1, respectively. The transmittances of the black and the white regions are 0 and 1, respectively. Namely, the incident beams are partly blocked by the black regions. Both of the counterpropagating incident cylindrical vector vortex beams experience the same amplitude modulations. These amplitude modulations can help to select appropriate angular spectrum to construct Poynting vector skyrmions with different topological invariants.

As shown in Fig. 4(a1), low spatial frequency components are selected and the focal electromagnetic fields oscillate slow in the focal plane within a prospective area,

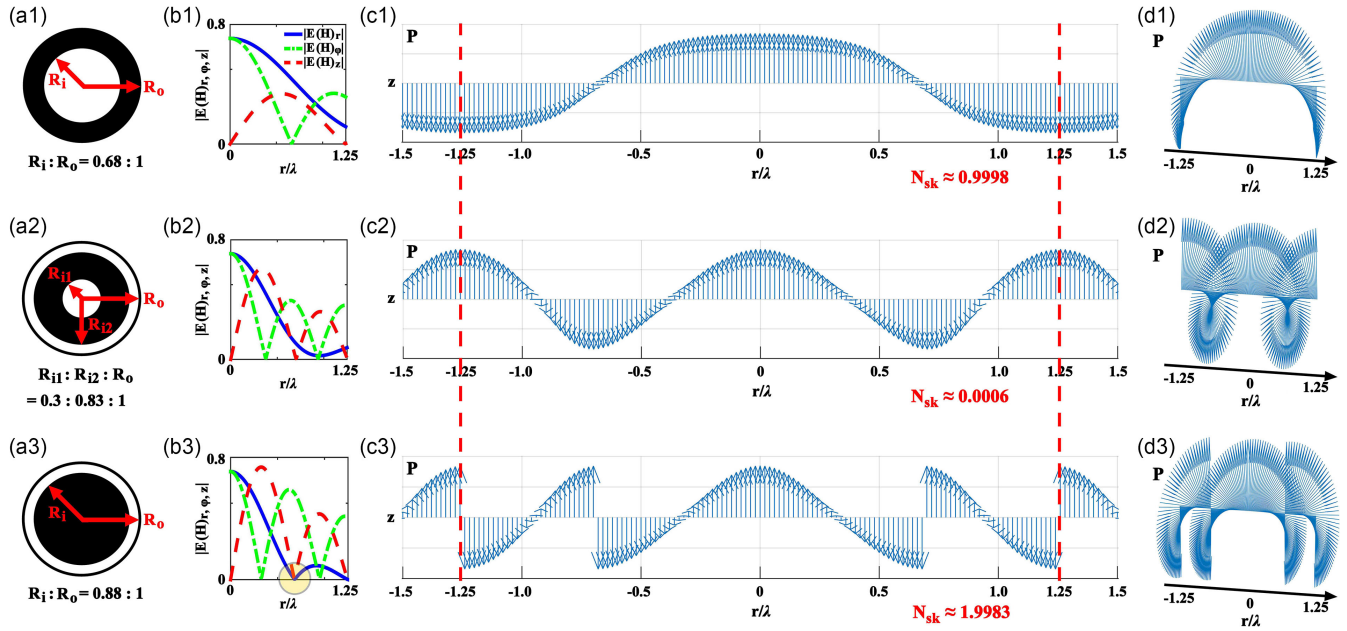


FIG. 4. Tuning the topological invariants of the Poynting vector skyrmion in a prospective area by modulating the amplitude of the incident beams. (a1)–(a3) The amplitude modulation of the incident beams. The transmittances of the black and the white regions are 0 and 1, respectively.  $R_0$  is the radius of the back aperture of the focal lenses.  $R_1$ ,  $R_{11}$ , and  $R_{12}$  are the inner radii of the amplitude modulation rings. (b1)–(b3) The cross sections of  $|E(H)_{r,\varphi,z}|$  in the focal plane, which are normalized to  $|E_f|$  or  $|H_f|$ . The radius of the prospective area is set to  $1.25\lambda$ . (c1)–(c3) The projections of the Poynting vector structures formed by unit vectors along the radial direction on the  $r$ - $z$  plane. The dashed red lines indicate the boundary of the prospective area. (d1)–(d3) The corresponding three-dimensional vectorial structures formed by unit vectors along the radial direction.

the radius of which is set to  $1.25\lambda$  as shown in Fig. 4(b1). The cross sections are normalized to  $|E_f|$  or  $|H_f|$ . In this case, only one singular point of  $E_\varphi(H_\varphi)$  and two singular points of  $E_z(H_z)$  appear within the prospective area, and accordingly a Bloch type Poynting vector skyrmion is generated. The projections of the Poynting vector structures formed by unit vectors along the radial direction on the  $r$ - $z$  plane are shown in Fig. 4(c1). It can be seen that within the prospective area indicated by the dashed red lines, the topological invariant of the Poynting vector skyrmion is approximately 1. The corresponding three-dimensional vectorial structure is shown in Fig. 4(d1). Then, higher spatial frequency components are added as modulated by Fig. 4(a2). In this case, the oscillation frequency of  $E_z(H_z)$  is doubled and one more singular point of  $E_\varphi(H_\varphi)$  appears, which generate a Bloch type Poynting vector skyrmion with a topological invariant of around 0 as the unit vectors rotate back to the “up” state at the periphery as shown in Figs. 4(b2), 4(c2), and 4(d2). Beyond the prospective area, a skyrmionium structure (nested Poynting vector skyrmion) can be noticed as the topological invariant changes between 1 and 0 in the entire focal plane. By further increasing the proportion of high spatial frequency components as shown in Fig. 4(a3), a singular point of  $E_r(H_r)$  appears in the same position with that of  $E_z(H_z)$  as indicated by the yellow shaded area in Fig. 4(b3). This special point leads to a phase jump, namely the singularity of Poynting vectors. Across

this point, Poynting vectors reverse orientations as shown in Figs. 4(c3) and 4(d3), which results in a topological invariant of around 2 within the prospective area. Beyond the prospective area, the topological invariant increases monotonically as the singularity of Poynting vectors appears regularly in the entire focal plane. The corresponding evolutions of the phase distributions and local singularities along the propagating direction, which are similar to the changing regularity presented by Fig. 3, are shown in Fig. S4 [51]. This tunable feature by beam modulations opens new avenues of fine and dynamic configuring of optical skyrmion textures in the focal region. It is worth noting that more systematic and complicated skyrmion structures are obtainable through further amplitude, phase, or polarization modulations.

In summary, as a new family member of optical skyrmions, Poynting vector skyrmions are constructed in the focal region of two pairs of counterpropagating cylindrical vector vortex beams in free space. Through analyzing the variations of the vortex phases and the phase singularities of the individual components of the focal electromagnetic field along the light propagating direction, a Néel-Bloch-Néel transition of Poynting vector skyrmion textures has been observed. By further modulating the amplitude of the incident beams, the skyrmion number of the Poynting vector skyrmions can be tuned in a prospective area. We envision that these theoretical results may expand the

research scope of topological photonics and hold potentials to realize energy flow associated applications such as optical trapping, particle manipulation, and beam steering.

*Acknowledgments*—This research is financially supported by the National Key R&D Program of China (2021YFB2802003, 2023YFF0718101), National Natural Science Foundation of China (NSFC) (62375109, 61975066, 62075084, 62075085, 62005104), Guangdong Basic and Applied Basic Research Foundation (2021A1515011586, 2020A1515010615, 2020B1515020058, 2022B1515020004), Guangzhou Science and Technology Program (2024A03J0465).

- [1] T. H. R. Skyrme, *Nucl. Phys.* **31**, 556 (1962).
- [2] J. Ruostekoski and J. R. Anglin, *Phys. Rev. Lett.* **86**, 3934 (2001).
- [3] U. Al Khawaja and H. Stoof, *Nature (London)* **411**, 918 (2001).
- [4] J. Fukuda and S. Žumer, *Nat. Commun.* **2**, 246 (2011).
- [5] S. Mühlbauer, B. Binz, F. Jonietz, C. Pfleiderer, A. Rosch, A. Neubauer, R. Georgii, and P. Böni, *Science* **323**, 915 (2009).
- [6] X. Z. Yu, Y. Onose, N. Kanazawa, J. H. Park, J. H. Han, Y. Matsui, N. Nagaosa, and Y. Tokura, *Nature (London)* **465**, 901 (2010).
- [7] N. Romming, C. Hanneken, M. Menzel, J. E. Bickel, B. Wolter, K. Bergmann, A. Kubetzka, and R. Wiesendanger, *Science* **341**, 636 (2013).
- [8] N. Nagaosa and Y. Tokura, *Nat. Nanotechnol.* **8**, 899 (2013).
- [9] I. Kézsmárki, S. Bordács, P. Milde, E. Neuber, L. M. Eng, J. S. White, H. M. Rønnow, C. D. Dewhurst, M. Mochizuki, K. Yanai, H. Nakamura, D. Ehlers, V. Tsurkan, and A. Loidl, *Nat. Mater.* **14**, 1116 (2015).
- [10] Y. Shen, Q. Zhang, P. Shi, L. Du, A. V. Zayats, and X. Yuan, *Nat. Photonics* **18**, 15 (2024).
- [11] S. Tsesses, E. Ostrovsky, K. Cohen, B. Gjonaj, N. H. Lindner, and G. Bartal, *Science* **361**, 993 (2018).
- [12] T. J. Davis, D. Janoschka, P. Dreher, B. Frank, F. Heringdorf, and H. Giessen, *Science* **368**, eaba6415 (2020).
- [13] C. Bai, J. Chen, Y. Zhang, D. Zhang, and Q. Zhan, *Opt. Express* **28**, 10320 (2020).
- [14] Y. Shen, Y. Hou, N. Papisimakis, and N. I. Zheludev, *Nat. Commun.* **12**, 5891 (2021).
- [15] C. Liu, S. Zhang, S. A. Maier, and H. Ren, *Phys. Rev. Lett.* **129**, 267401 (2022).
- [16] L. P. Du, A. P. Yang, A. V. Zayats, and X. C. Yuan, *Nat. Phys.* **15**, 650 (2019).
- [17] X. Lei, A. Yang, P. Shi, Z. Xie, L. Du, A. V. Zayats, and X. Yuan, *Phys. Rev. Lett.* **127**, 237403 (2021).
- [18] X. Lei, L. Du, X. Yuan, and A. V. Zayats, *Nanophotonics* **10**, 3667 (2021).
- [19] P. Shi, L. Du, and X. Yuan, *Nanophotonics* **10**, 3927 (2021).
- [20] M. Lin, W. Zhang, C. Liu, L. Du, and X. Yuan, *ACS Photonics* **8**, 2567 (2021).
- [21] X. Lei and Q. Zhan, *ACS Photonics* **10**, 3551 (2023).
- [22] Y. Shen, E. C. Martínez, and C. Rosales-Guzmán, *ACS Photonics* **9**, 296 (2022).
- [23] H. Teng, J. Zhong, J. Chen, X. Lei, and Q. Zhan, *Photonics Res.* **11**, 2042 (2023).
- [24] Y. Shen, C. He, Z. Song, B. Chen, H. He, Y. Ma, J. A. J. Fells, S. J. Elston, S. M. Morris, M. J. Booth, and A. Forbes, *Phys. Rev. Appl.* **21**, 024025 (2024).
- [25] Y. Shen, B. Yu, H. Wu, C. Li, Z. Zhu, and A. V. Zayats, *Adv. Opt. Photonics* **5**, 015001 (2023).
- [26] A. Yang, X. Lei, P. Shi, F. Meng, M. Lin, L. Du, and X. Yuan, *Adv. Sci.* **10**, 2205249 (2023).
- [27] M. I. Tribelsky and B. S. Luk'yanchuk, *Phys. Rev. Lett.* **97**, 263902 (2006).
- [28] D. Gao, A. Novitsky, T. Zhang, F. C. Cheong, L. Gao, C. T. Lim, B. Luk'yanchuk, and C. Qiu, *Laser Photonics Rev.* **9**, 75 (2015).
- [29] A. Bekshaev, K. Bliokh, and M. Soskin, *J. Opt.* **13**, 053001 (2011).
- [30] M. E. J. Friese, J. Enger, H. Rubinsztein-Dunlop, and N. R. Heckenberg, *Phys. Rev. A* **54**, 1593 (1996).
- [31] O. V. Angelsky, M. P. Gorsky, P. P. Maksimyak, A. P. Maksimyak, S. G. Hanson, and C. Yu. Zenkova, *Opt. Express* **19**, 660 (2011).
- [32] A. Bekshaev, K. Bliokh, and M. Soskin, *J. Opt.* **13**, 053001 (2011).
- [33] X. Gao, Y. Pan, G. Zhang, M. Zhao, Z. Ren, C. Tu, Y. Li, and H. Wang, *Photonics Res.* **5**, 640 (2017).
- [34] Z. Man, Z. Bai, S. Zhang, X. Li, J. Li, X. Ge, Y. Zhang, and S. Fu, *Opt. Express* **26**, 23935 (2018).
- [35] X. Jiao, S. Liu, Q. Wang, X. Gan, P. Li, and J. Zhao, *Opt. Lett.* **37**, 1041 (2012).
- [36] V. V. Kotlyar, A. A. Kovalev, and A. G. Nalimov, *Opt. Lett.* **43**, 2921 (2018).
- [37] V. V. Kotlyar, S. S. Stafeev, and A. G. Nalimov, *Opt. Express* **27**, 16689 (2019).
- [38] V. V. Kotlyar, S. S. Stafeev, and A. G. Nalimov, *Phys. Rev. A* **99**, 033840 (2019).
- [39] H. Wang, L. Shi, B. Luk'yanchuk, C. Sheppard, and C. Chong, *Nat. Photonics* **2**, 501 (2008).
- [40] G. Yuan, E. T. F. Rogers, and N. I. Zheludev, *Light Sci. Appl.* **8**, 2 (2019).
- [41] Y. Shen, N. Papisimakis, and N. I. Zheludev, *Nat. Commun.* **15**, 4863 (2024).
- [42] V. Kumar and N. K. Viswanathan, *Opt. Lett.* **38**, 3886 (2013).
- [43] E. J. Galvez, Vector beams in free space, in *The Angular Momentum of Light*, edited by D. L. Andrews and M. Babiker (Cambridge University Press, Cambridge, England, 2012), Vol. 3.
- [44] S. W. Jolly and M. A. Porras, *Opt. Lett.* **47**, 3632 (2022).
- [45] K. Huang, H. Ye, J. Teng, S. P. Yeo, B. Luk'yanchuk, and C. W. Qiu, *Laser Photonics Rev.* **8**, 152 (2014).
- [46] X. Hao, C. Kuang, T. Wang, and X. Liu, *Opt. Lett.* **35**, 3928 (2010).
- [47] B. Richards and E. Wolf, *Proc. R. Soc. A* **253**, 358 (1959).
- [48] W. Chen and Q. Zhan, *Opt. Lett.* **34**, 2444 (2009).
- [49] G. Chen, F. Song, and H. Wang, *Opt. Lett.* **38**, 3937 (2013).
- [50] S. Wang, Y. Cao, and X. Li, *Opt. Lett.* **42**, 5050 (2017).

- [51] See Supplemental Material at <http://link.aps.org/supplemental/10.1103/PhysRevLett.133.073802> for detailed formula derivations, purity of local Poynting vector components, normalized energy density of the focal electromagnetic field, schematic of the incident polarizations which are not mirror-symmetric, evolutions of the phase distributions and local singularities along the propagating direction after wave front shaping, which includes Refs. [47–50].
- [52] S. Wang, C. Wei, Y. Feng, Y. Cao, H. Wang, W. Cheng, C. Xie, A. Tsukamoto, A. Kirilyuk, T. Rasing, A. V. Kimel, and X. Li, *Appl. Phys. Lett.* **113**, 171108 (2018).